Stirring Effect on Bistability in a CSTR. 1. Experiments and Simulations for the AsO_3^{3-}/IO_3^- Reaction

Fathei Ali,[‡] Peter Strizhak,[†] and Michael Menzinger*[,‡]

Department of Chemistry, University of Toronto, Toronto, Ontario M5S 3H6, Canada, and L. V. Pisarzhevskii Institute of Physical Chemistry, National Ukrainian Academy of Sciences, pr. Nauki 31, Kiev, Ukraine 252038

Received: February 17, 1999; In Final Form: July 14, 1999

The effect of mixing-induced inhomogeneity on the bistability hysteresis of the arsenite−iodate reaction was studied experimentally in a CSTR, involving a single premixed feedstream, and by simulation using the coalescence−redispersion model. Conditions were chosen for which the system may be described by a single dynamical variable. It was found that reduced stirring causes the hysteresis loop to contract and to remain inside the high-stirring loop. The steady-state probability density functions were constructed from the fluctuating time series and were found to be gaussian. They represent the stochastic description of the macroscopic stirring effect. The agreement of experiments and simulations confirms the micromixing scenario and the appropriateness of the mixing model.

1. Introduction

While traditional chemical kinetics deals with homogeneous systems, the study of stirring effects[1,2] has shown that, in flow reactors, the ideally mixed, homogeneous limit is often not achieved and that inhomogeneities which survive the mixing process may sensitively affect the kinetics and dynamics of nonlinear reactions. Reactive flows become homogeneous in the limits of fast mixing and slow reaction and flow, but the condition of fast mixing is frequently not fulfilled in real systems such as the atmosphere, the ocean, industrial reactors, and biological systems. It is important, therefore, to understand qualitatively and quantitatively the dynamic consequences of different reactor inhomogeneities and to develop approaches for predicting the effects of inhomogeneity in different classes of kinetic systems.

The dynamics of a flow reactor, e.g., a CSTR, is determined both by the chemical reaction mechanism and by its hydrodynamic state. The latter may be manipulated by the mixing mode M and by the stirring rate S.[3,4] The role of these experimental variables is sometimes referred to as stirring and mixing (S&M) effects.[2] Mixing mode refers to the premixed (PM) or nonpremixed (NPM) configuration of feedstreams.[3,4,6,7] Because S&M responses arise from the nonlinear coupling of turbulent flow with chemical relaxation, they depend on the chemical mechanism. Little is known to date about the role of the reaction mechanism on S&M effects.

The reactor inhomogeneity, one object of our study, manifests itself through concentration fluctuations. In fast nonlinear reactions, the rate, steady-state concentrations, and fluctuations may be manipulated through the stirring rate and mixing mode.[3,4] When chemical instabilities are present, e.g., in oscillating and bistable media, oscillation attributes (frequency and amplitude) and the location of bifurcation points also depend on S and M. Another kind of stirring effect is the chiral symmetry breaking in crystal precipitation from a stirred medium.[8] The CSTR inhomogeneitiy arises primarily from the incomplete mixing of feedstreams with each other and/or with the reactor bulk[6] rather than from the nucleation process associated with a nonequilibrium phase transition.[3,9]

Hence, the effects of the mixing-induced inhomogeneity may be readily simulated using a variety of mixing models described in the chemical engineering literature.[2,10] In *macromixing models*, the essential inhomogeneity consists of differently mixed, macroscopic subvolumes, and the primary effect of this inhomogeneity is to change the reactor's residence time distribution from its ideal, exponential limit. The coupled-reactor models that fall within this class describe the mixing process by linear coupling of two or more weakly connected reactor compartments.[2,11−15] *Micromixing models*,[2,5] on the other hand, allocate the essential inhomogeneity to the turbulent eddies that result from the turbulent mixing or Kolmogorov cascade.[16] These eddies are finally dissipated by turbulent diffusion. This process may be described by a mean-field approach.[17] Alternatively, the random nature of the mixing process may be retained explicitly, e.g., in the coalescence−redispersion (CR) model,[10] which provides a probabilistic description of the mixing process. We will employ it in this work. *Computational fluid dynamics* is the most detailed and computation intensive approach to fluid mixing,[18] and it goes beyond the requirements of the present problem.

The CR model assumes that the CSTR is composed of a collection of N independently evolving cells. To mimick the flow, randomly chosen cell(s) are replaced periodically with fresh reactants. Mixing is achieved by equalizing the concentrations in pairs of randomly chosen cells by coalescing and redispersing them at a rate different from that of the flow. At any moment, the state of the CSTR is given by the concentration distribution over the cells, from which the probability density function (pdf) may be readily obtained.[19] In this and the companion paper,[20] the CR model is employed to simulate and interpret the experimental data.

Elsewhere, we analyzed the stirring effect on a generic one-variable model of chemical bistability[21] and showed that a

* To whom correspondence should be addressed. E-mail: menzinger@chem.utoronto.ca.
† University of Toronto.
‡ National Ukrainian Academy of Sciences.

10.1021/jp9906029 CCC: $18.00 © 1999 American Chemical Society
Published on Web 11/18/1999

decreased rate of stirring causes the hysteresis to contract along both directions, so that the upper and lower steady states as well as the critical values of the control parameters approach each other and the low-S hysteresis loop is entirely contained in the high-S loop. We called this response a *stirring effect of the first kind*. Systems that respond otherwise exhibit a *stirring effect of the second kind*. Real systems that exhibit a stirring effect of the first kind, although they are known to involve more that one dynamical variable, are *effectively one-dimensional*. Known examples are the chlorite−iodide reaction,[3,4,6,22,23] the BZ reaction,[21,24] and the arsenite−iodate reaction studied in this paper. Stirring effects of the second kind were found in the Briggs−Rauscher reaction[25,26] and in the minimal bromate reaction.[7,27]

The aims of this paper are to experimentally study the bistable arsenite-iodate reaction which involves a single variable when arsenite is in excess,[28,29] by comparing laboratory experiments and computer simulations based on the CR model. By monitoring the reaction on a small length scale of ~40 μm with a Pt microelectrode and analyzing the resulting fluctuating time series, we obtained the pdf, which is a more informative measure of the stochastic state of the CSTR than the average signal. The shift $\Delta = x_s - x_d$ of the stochastic average from the deterministic, high-stirring limit and the shift of the transition points are referred to as the *macroscopic stirring effects*. The data analysis involves comparing the probability density functions and the first two moments of the fluctuating signal. The good agreement confirms the essential validity of the CR model. Although the analysis based on pdf is more revealing than the standard approach based on averages, it does not provide the kind of physical insight obtainable from analytical theory. Therefore, in the companion paper,[20] we derive an analytical version of the CR model, based on stochastic differential equations.[26,30−33] It provides explicit expressions for the stochastic steady states (the first moments) and for the connection of the macroscopic stirring effect Δ with the reactor inhomogeneity (the second moment of the pdf), and hence physical insight into the sources of fluctuations and the stirring effect.

The experimental procedure and results are summarized in sections 2a and 2b. The data consist of average potential (first moment), the variance (second moment), and the complete pdf, as functions both of in-flow concentration $[I^-]_0$ and of stirring rate S. The CR model is described in section 3a, and the results of simulations are compared with experimental results in section 3b. These are discussed in the final section 4.

2. Experiments

2.1. Experimental Procedure. Experiments were conducted in a cylindrical plexiglass CSTR (inner diameter, 31 mm; volume, $V = 28$ mL),[7,22] thermostated at $T = 25$ °C. The rectangular impeller (8 × 15 mm stainless steel coated with Teflon) was positioned 30 mm above the bottom of the reactor. The CSTR was equipped with four baffles to enhance turbulence.[2] The stirring rate could be varied from $S = 0$ to 1500 rpm. The state of the system was monitored by a Pt microelectrode (20 μm diameter Pt wire fused in glass, trimmed to ~30 μm length), located near the stirrer, relative to a $Hg/HgSO_4$ reference electrode. The impedance-matched electrode signal was fed via an A/D converter into a personal computer.

The iodide feedstream concentration $[I^-]_0$ was chosen as the control parameter because it alters only the chemical rate without also affecting the hydrodynamic state. Two identical reactant feedstreams were peristaltically pumped into the reactor through two ports, located on opposite sides of the reactor just below the stirrer, at a constant rate of 2.4 mL/min, corresponding to a residence time $\tau_{flow} = 233$ s. Three reagent solutions were used: (1) 2.1×10^{-3} M KIO_3; (2) 1.0×10^{-2} M $NaAsO_2$ and 1.0×10^{-2} M H_2SO_4; (3) the third solution contained sodium iodide whose concentration $[I^-]_0$ was used as the control parameter. In addition, each solution contained 0.05 M Na_2SO_4 and 0.05 M $NaHSO_4$ as a buffer (pH = 2.1). Feedstreams 2 and 3 were premixed and subsequently combined with feedstream 1 in two T-shaped capillary tubes just prior to entering the reactor.

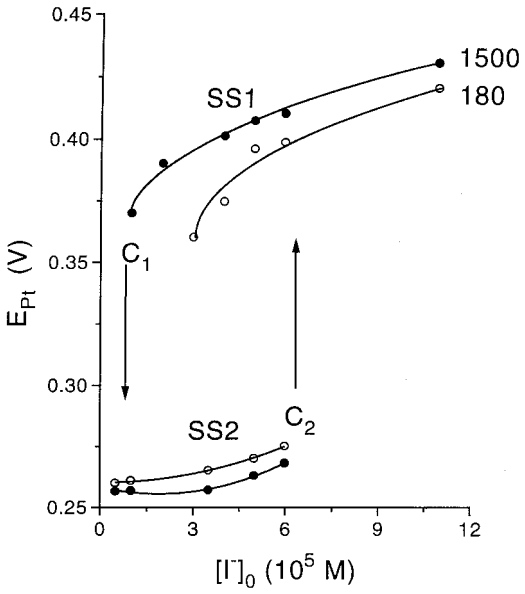

Figure 1. Experimental dependence of the system response (time average of the Pt-electrode signal) on the control parameter for two stirring rates: open circles, 180 rpm; filled circles, 1500, rpm. Autocatalysis is switched on on SS1 and off on SS2.

The hysteresis was mapped out as a function of $[I^-]_0$ and of S, and the dependence of the fluctuating signal on stirring rate was analyzed by computer. The coarse-grained pdf, normalized to unity, was constructed by sorting the values of a fluctuating Pt-electrode signal into appropriately chosen bins and counting the population of each bin. The first and second moments of the fluctuating signal were calculated using the standard statistical approach.

2.2. Experimental Results. Figure 1 shows the hysteresis at two different values of the stirring rate S. The state of the system is characterized by the average value of the Pt potential. At high $[I^-]_0$, the system resides in steady state SS1, characterized by high values of electrode potential, a high concentration of iodide ions, and autocatalysis switched on. Starting at high values of $[I^-]_0$, the system remains in SS1 down to the critical value x_1. At x_1 the system jumps to the second branch of steady state SS2, characterized by low values of the potential, low iodide concentrations and autocatalysis switched off. Scanning $[I\text{-}]_0$ in the opposite direction induces the reverse transition from SS2 to SS1 at the second critical concentration x_2. Thus, two steady states coexist between x_1 and x_2. At reduced stirring the hysteresis loop contracts in both directions as follows: SS1 shifts down toward SS2, and SS2 shifts up toward SS1. At the same time, the critical point x_1 shifts toward x_2, i.e., to higher concentrations of iodide in the inflow. On the lower branch, the stirring effect is less pronounced and the change of x_2 was not resolved.

Figure 2 represents the corresponding fluctuation amplitude, given as the standard deviation σ^2 of the Pt-electrode potential.

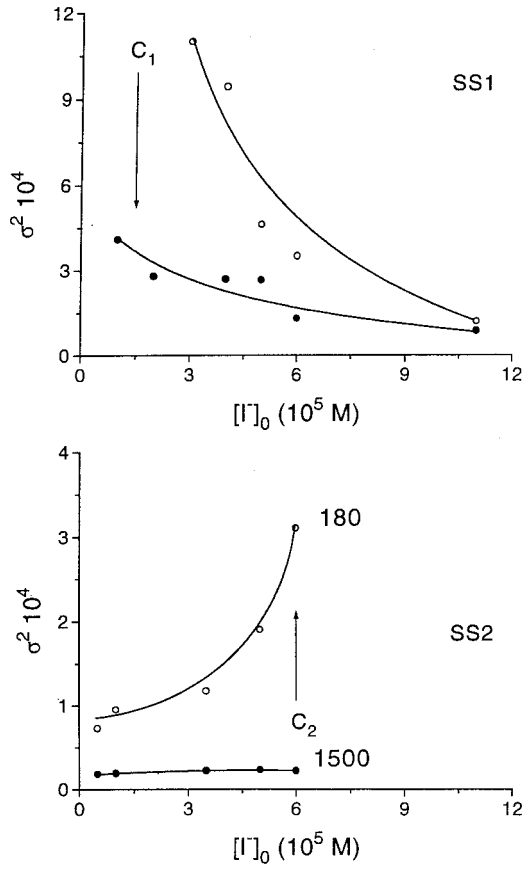

Figure 2. Experimental dependence of the noise (variance of the Pt-electrode signal) on the control parameter for two stirring rates. Symbols are as in Figure 1. Arrows indicate critical values of the control parameter and transitions.

As the transition points are approached, the fluctuations increase on both branches. The fluctuation amplitude also increases on both branches with decreasing stirring rate and fixed $[I^-]_0$.

The data presented in Figures 1 and 2 illustrate the effect of stirring on the first and second moments of the fluctuating signal. A more general description of the underlying stochastic reality is given by the pdf, i.e., the probability of finding the system in a state characterized by a certain value of the electrode potential. Figure 3 shows the probability density functions, constructed from the fluctuating signals for both steady states at two values of the stirring rate. The pdf's are Gaussian. As S decreases, the pdf's become broader and move toward each other. This is the stochastic representation of the fact that the hysteresis shrinks with decreasing stirring, i.e., of the *stirring effect of the first kind*.[21]

3. Simulations

3.1. The Coalescence−Redispersion Model. The mixing model used to analyze the stirring effects was introduced by Curl[10] and is known as the CR model. It was widely applied to chemical engineering problems,[32−35] and its Monte Carlo version was first described by Spielman and Levenspiel.[33] Horsthemke and Hannon used it to analytically describe the mixing effect in one-dimensional systems with cubic autocatalysis,[30] and in a two-dimensional model of the arsenite−iodate reaction.[31]

In the CR model, the CSTR is considered to be composed of a large number N (here $N = 800$) of identical cells. In each cell the concentration may change because of mixing, reactant flow, or chemical relaxation as follows. *Mixing* is represented by the collisions of randomly chosen pairs of cells that take place at fixed time intervals $\Delta\tau_m$. It results in the averaging ("coalescing and redispersing") of concentrations in the two cells according to

$$x_i = x_j = (x_i + x_j)/2 \tag{1}$$

On average, it takes $\tau_{mix} = N\Delta\tau_m/2$ time units, the characteristic mixing time, for a given cell to undergo one mixing event. To represent the *flow*, a randomly chosen cell is replaced with a feedstream cell with concentration x_0 at regular intervals $\Delta\tau_f$. The feeding interval $\Delta\tau_f$ is related to the residence time by $\tau_{flow} = 1/k_{flow} = N\Delta\tau_f$ when a single, premixed feedstream is used. *Chemical relaxation* occurs between the feeding and mixing events, and the content of each cell evolves according to the rate law

$$dx_i/dt = f(x_i) \tag{2}$$

where $f(x)$ represents the batch rate.

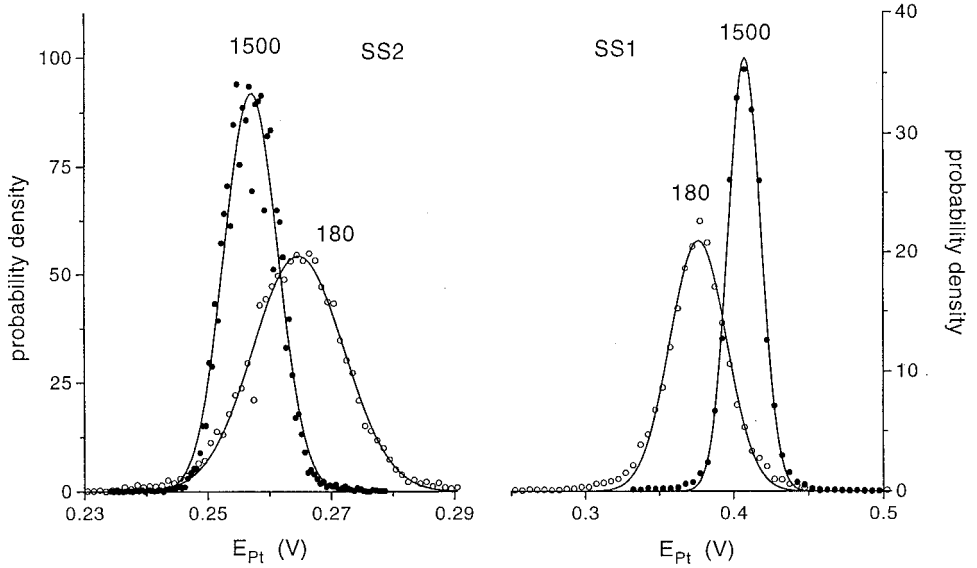

Figure 3. Experimental pdf of the electrode potential at two different stirring rates (rpm) for both branches, $[I^-]_0 = 3.5 \times 10^{-5}$ M. Symbols are as in Figure 1.

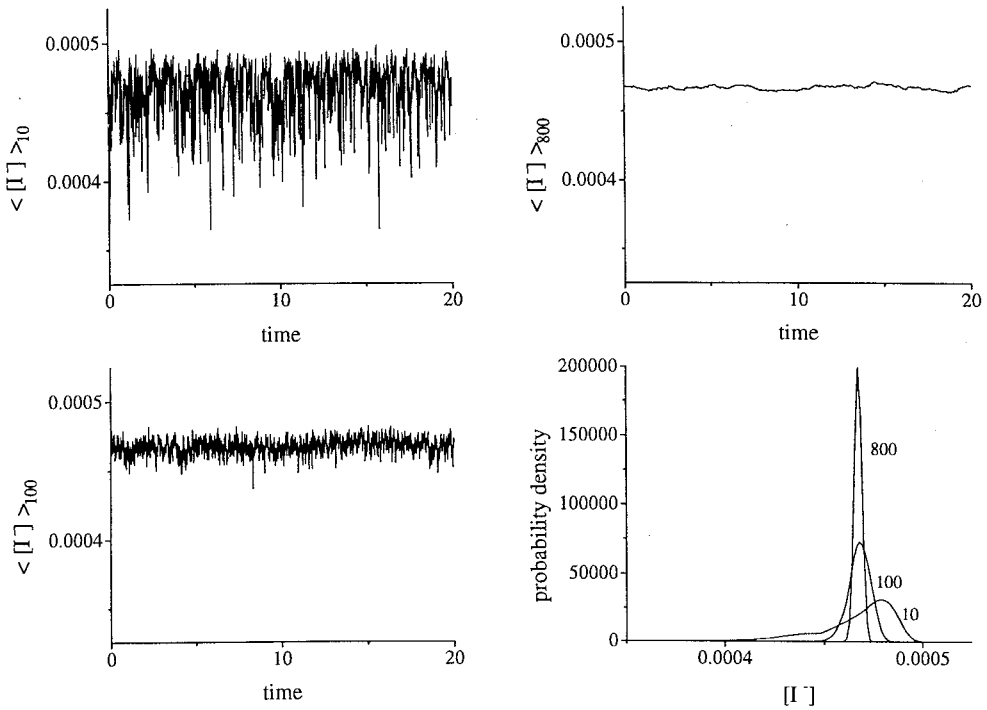

Figure 4. Stochastic time series and corresponding pdf obtained from simulations by the CR model. Averaging is performed over the entire reactor $\langle I^- \rangle_{800}$, over 100 cells $\langle I^- \rangle_{100}$, and over 10 cells $\langle I^- \rangle_{10}$, with $\tau_{mix} = 0.0533$, $\tau_{flow} = 1.6$, and $[I^-]_0 = 8 \times 10^{-5}$ M.

3.2. Kinetic Model. When arsenous acid is in stoichiometric excess, the net reaction is given by[36]

$$IO_3^- + 3H_3AsO_3 = I^- + 3H_3AsO_4$$

and its empirical rate law is[37]

$$\frac{d[I^-]}{dt} = -\frac{IO_3^-}{dt} = (k_1 + k_2[I^-])[I^-][IO_3^-][H^+]^2 \quad (3)$$

where I^- acts as the autocatalyst. In this case the reaction rate no longer depends on $[AsO_3^{3-}]$ and the system behaves effectively as one-dimensional.[36] Accordingly, the rates of change of iodide and iodate concentrations are related by

$$\frac{d[I^-]}{dt} + \frac{d[IO_3^-]}{dt} = 0$$

This implies the following conservation condition for each cell

$$[I^-] + [IO_3^-] = [I^-]_0 + [IO_3^-]_0 \quad (4)$$

where $[I^-]_0$ and $[IO_3^-]_0$ are the inflow concentrations. It allows one to reduce from a two-variable to a single-variable rate law. It is fulfilled only if both reactants are supplied in a single, premixed feedstream. Therefore, the present study is confined to the PM feedstream configuration. Combining eqs 3 and 4 yields the one-variable rate law

$$dx/dt = f(x) = (k_1 + k_2x)(y_0 + x_0 - x)[H^+]^2x$$
$$= -k_2h^2x^3 + [(x_0 + y_0)k_2 - k_1]h^2x^2 + (x_0 + y_0)h^2k_1x \quad (5)$$

where $x = [I^-]$, $x_0 = [I^-]_0$, $y_0 = [IO_3^-]_0$ and $h = [H^+]$. The rate constants are $k_1 = 4.5 \times 10^3$ M^{-3} s^{-1} and $k_2 = 4.5 \times 10^8$ M^{-4} s^{-1}.[36] We chose the remaining parameters to lie in the bistable range of the model, i.e., $[H^+]_0 = 0.1$ M, $[IO_3^-]_0 = 7.4 \times 10^{-4}$ M, and $\tau_{flow} = 1/k_{flow} = 1.6$ s. As in the experiment, the inflow concentration of iodide $[I^-]_0$ was chosen as the control parameter. In the limit $\tau_{mix} = 0$, the CSTR kinetics is governed by the deterministic rate law

$$dx/dt = f(x) + k_{flow}(x_0 - x) \quad (6)$$

Depending on the value of $[I^-]_0$, this equation has either one or three steady states.

3.3. Analysis of Results. The state of the reactor is fully described by the concentration vector of iodide $\mathbf{x}(t) = \{x_1(t), ..., x_i(t), ..., x_N(t)\}$ in all cells. These concentrations fluctuate because of the processes of mixing and flow. An experimental observable is related to the average concentration $x_M(t)$ over $M \leq N$ cells, where M is a measure of the sampling volume:

$$x_M(t) \equiv \langle x(t) \rangle_M = 1/M \sum_{i=1}^{M} x_i(t) \quad (7)$$

If $M = N$, this gives the average concentration $x_N(t)$ of the entire reactor. The time series of $x_N(t)$ and $x_M(t)$ are presented in Figure 4a−c for $M = 800$, 100, and 10. The noise of the signal increases with decreasing sampling volume M. Figure 4d represents the corresponding pdf's calculated from these signals. The coarse-grained probability density $P(x_M)$ is constructed by sorting the time series $x_M(t)$ into appropriately chosen concentration bins and equating the fraction of cells in the bin with central coordinates x to $P(x_M)$. Typically, 50 bins were used. The pdf is almost gaussian if averaging is performed over the entire reactor or over a sufficiently large number of cells (Figure 4d; $M = 800$ and 100), while averaging over a small number of cells (Figure 4d; $M = 10$) produces a noticeably asymmetric probability distribution. In the experiments we observed only gaussian pdf (Figure 3), even with a Pt micro-

electrode and at the lowest stirring rates. This may be due to the fact that the electrode is fixed in space and that it does not sample the more inhomogeneous subvolumes. In particular, the probability of sampling freshly injected subvolumes (the reason behind the asymmetry of the computed pdf) is very small. Another possibility is that the spatial scale of the asymmetry may be smaller than the size of the microelectrode, and substantial spatial averaging may occur even on the microelectrode. A third possibility is that time averaging may come into play because of the finite response times of electrode and electronics.

The steady states are taken to be the time averages of $x_N(t)$[38]

$$\bar{x} = 1/T\int_0^T x_N(t)\,\mathrm{d}t \tag{8}$$

Shown by the circles in Figure 5 are the computed values of $\bar{x}$ at different inflow iodide concentrations for two different mixing times. The solid line represents the deterministic steady states. On the scale of this figure, the lower stochastic state SS2 cannot be distinguished from the deterministic branch. However, with higher resolution, e.g., in Figure 7, the upward shift of the computed averages at decreased stirring is clearly visible. The results indicate that, for a finite value of τ_{mix}, the stochastic SS1 is always lower than the deterministic steady state, while SS2 always lies higher than its deterministic limit. The shift Δ is pronounced for SS1, but the calculated shift of SS2 is smaller than that in the experiment; see Figure 1. Increasing τ_{mix} shifts the left hysteresis limit to the right and the right limit to the left, while SS1 always shifts down and SS2 shifts up. Therefore, in response to increased τ_{mix}, the hysteresis shrinks in both directions.

The level of fluctuations that reflects the reactor inhomogeneity is given by the second moment

$$\sigma^2 = \overline{\langle (x_i(t) - x_N(t))^2 \rangle_N}$$
$$= \frac{1}{T}\int_0^T \frac{1}{N}\sum_{i=1}^{N} (x_i(t) - x_N(t))^2\,\mathrm{d}t \tag{9}$$

Figure 6 presents the calculated dependence of the relative second moment $\sigma^2/\bar{x}^2$ on the control parameter for both steady states. To see that this relative value corresponds to fluctuations of the Pt-microelectrode potential, note that the electrode potential is proportional to the logarithm of the concentration $E_{pt} \sim \log x$ and that its absolute variation is proportional to the relative variation of the concentration $\delta E_{Pt} = \delta x/\bar{x}$. This (relative) noise intensity increases near both hysteresis limits, in agreement with the experimental results in Figure 2. It should be emphasized that, in contrast, the *absolute* concentration fluctuation δx *decreases* on SS1 as x_1 is approached, while it *increases* on SS2 as x_2 is approached. The decrease of δx near x_1 confirms that the fluctuations do not arise from nucleation.[3,9] The issue of the evolution of fluctuations near the bistability limits will be taken up elsewhere. In this paper and in part 2, we discuss only the stirring dependence of the first moment $\bar{x}$ and of the second moment (the reactor inhomogeneity) σ^2.

The stochastic state of the reactor is characterized more fully by its probability density function. The computed pdf's are plotted in Figure 7 for both steady states at two values of τ_{mix}. They are similar to the measured distributions in Figure 3. The correspondence between the experimental data in Figures 1−3 and the simulations in Figures 5−7 is remarkable. It indicates that the CR model adequately describes the stirring dependence of steady states, hysteresis limits, and fluctuation amplitudes in the arsenite−iodate reaction, if arsenous acid is in excess, i.e., if the reaction behaves effectively as one-dimensional.

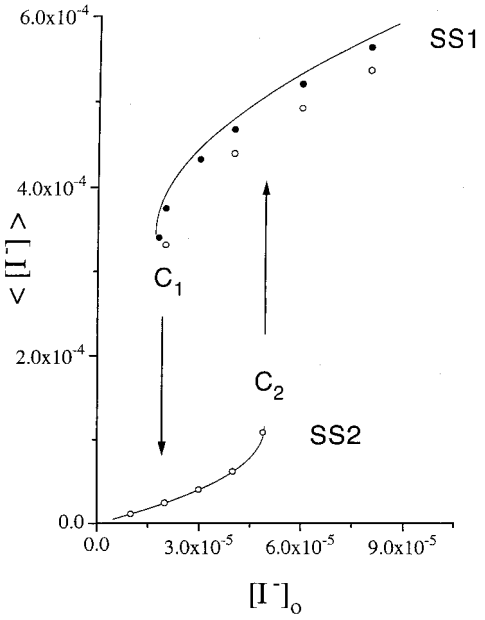

Figure 5. Response diagram calculated from the CR model. Lines represent the deterministic response diagram calculated from eq 6. Filled circles represent the stochastic response at rapid mixing $\tau_{mix} = 0.016$ s and open circles at slow mixing $\tau_{mix} = 0.0533$ s. On the scale of the figure, the response on SS2 at the two mixing rates is not resolved, and only one data set (open circles) is shown. The shifts Δ of the stochastic steady states from the deterministic, high-stirring limit, will be analyzed quantitatively in part 2.[20]

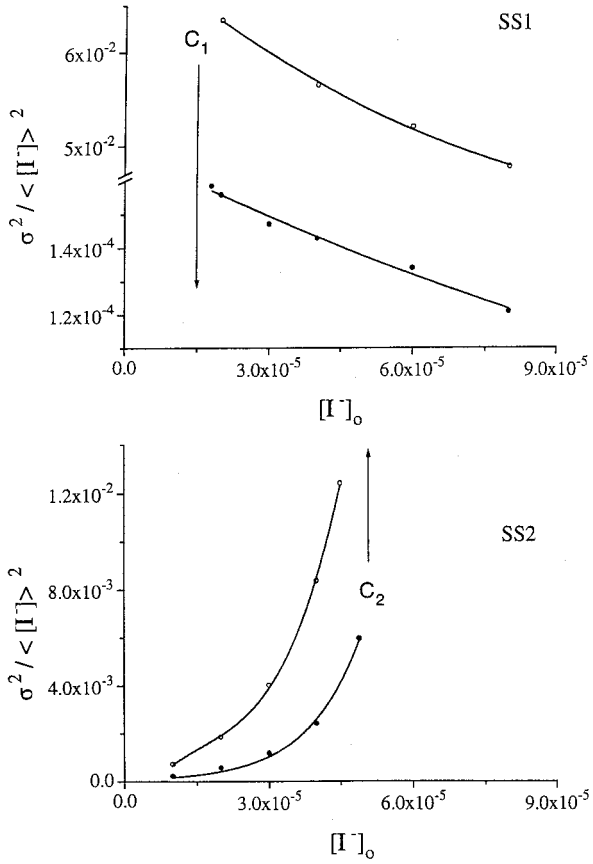

Figure 6. Dependence of the relative second moment on the control parameter at $\tau_{mix} = 0.0533$ by the CR model. Symbols are as in Figure 1.

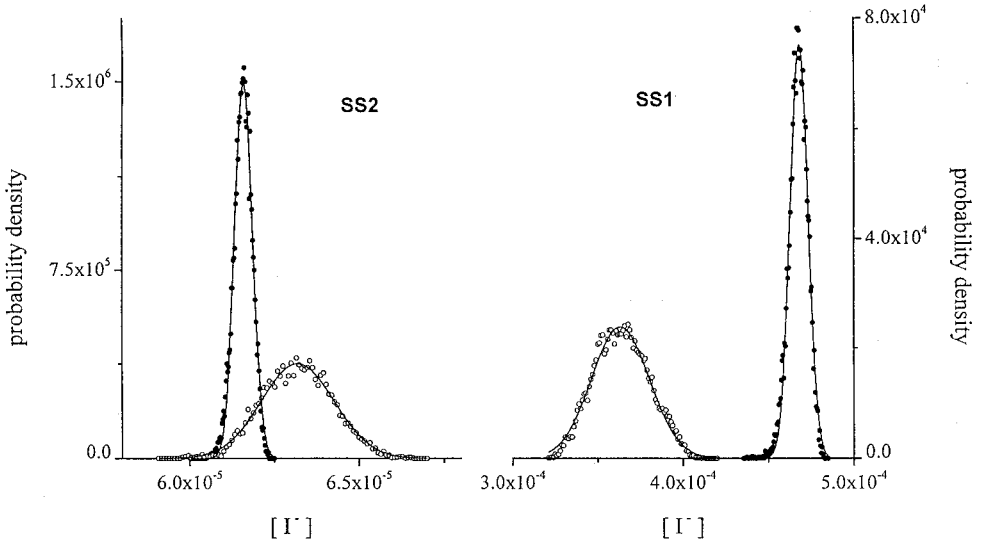

Figure 7. Probability distribution function of the iodide concentration at two values of the mixing time (0.0533 and 0.016 s) for both branches, at $[I^-]_0 = 4 \times 10^{-5}$ M, calculated by the CR model. Symbols are as in Figure 1.

4. Discussion

As expected, the experiments show that the bistable, one-variable arsenite−iodate system exhibits a stirring effect of the first kind. Qualitatively, the simulations agree fully with the experimental results, but the agreement is not perfect. First, the kinetic model does not exhibit bistability for the parameter values used in experiment. Second, the functional dependence of mixing time τ_{mix} on the stirring rate S and residence time τ_{flow} is not known. By assuming that they are inversely related by $\tau_{mix} \sim S^{-1}$, however, we show in part 2[20] that the experimental and calculated stirring effects Δ scale linearly with σ^2 and that both depend linearly on stirring and mixing rates, S^{-1} and τ_{mix}^{-1}, respectively. Third, the relationship between the Pt-electrode potential and the concentration of iodide ions is not obvious. Hence, we discuss in this paper only qualitative aspects of the experimental and numerical results and reserve their quantitative analysis for part 2.[20] The experiments and simulations agree on two levels: on a deterministic level, the shift Δ of the steady state and the shift of the bifurcation points from the homogeneous, high-stirring limit (Figures 1 and 5); on a stochastic level, the pdf of the fluctuating signal (Figures 3 and 4d) and its second moments (Figures 2 and 6).

To understand qualitatively how reactor inhomogeneity causes the two steady states to shift in opposite directions, consider first the case of a reaction with a one-term nonlinear rate law, e.g., $dx/dt = kx^n$, $n > 1$. For this case, the rate $\langle x^n \rangle$ averaged over all subvolumes is always greater than the rate $\langle x \rangle^n$ of the average (homogeneous) reactor:

$$\langle x^n \rangle > \langle x \rangle^n$$

i.e., the inhomogeneity *enhances* the average rate. The higher the degree of nonlinearity n, the stronger is the enhancement. Now consider the rate function given by eq 5 containing two nonlinear terms with opposite sign. The net effect of inhomogeneity is now the combined effect of these two terms. On the low-$[I^-]$ branch, the effect of the quadratic, positive term outweighs the negative contribution of the cubic term; hence, the net rate is slightly enhanced. On the high-$[I^-]$ branch, however, the overall rate is sharply reduced because of bigger contribution of the cubic, negative term. This qualitative argument will be quantified in part 2,[20] where we show that the effect of inhomogeneity on rate and steady states is governed by the second derivative f'' of the rate function.

In its simplest form, mixing may be represented by coupled-reactor, macromixing models.[11,12] While sharp concentration gradients are certainly present at the inflow ports, the present work provides compelling evidence that a micromixing point of view is more appropriate. While inhomogeneities of any kind, be they microscopic or macroscopic, cause the steady-state concentrations to shift and the bifurcation set to be displaced, it is only the agreement on the pdf or stochastic level that provides direct evidence of the true spatiotemporal nature of the inhomogeneities. The results represent clear evidence of micromixing as the dominant physical cause of the observed stirring effect, with turbulent eddies as the elementary units. These eddies arise in the mixing process as the blobs of incoming, unmixed fluid undergo a stretching and folding or fractalization process until the size of the objects reaches the Kolmogorov limit.[16] This evolution of turbulent eddies is described by the CR model whose basic assumptions are as follows:[5,30] (i) The size of cells does not depend on the stirring rate (mixing time). Cells represent turbulent eddies, whose size for isotropic turbulence is given by[16] $\lambda = \bar{u}^3/\epsilon$. Here $\bar{u}$ is the root-mean-square velocity and ϵ is the rate of energy dissipation. The dissipation length λ is independent of the stirring rate S because $\bar{u}$ scales linearly with S and ϵ scales as the cube of S.[39] (ii) The probability of coalescence with any other cell is the same for each cell and independent of time, chemical composition, or location in a CSTR. (iii) Redispersion occurs immediately after coalescence; i.e., the characteristic time scale of redispersion is much smaller than the other characteristic times τ_{flow}, τ_{chem}, and τ_{mix}. It follows from these assumptions that the CR model is expected to fail at low stirring rates where it no longer describes realistically the eddies evolution and the molecular diffusion processes that begin to dominate. For instance, we found bimodal pdfs in experiments at $S = 40$ rpm, a phenomenon that cannot be explained in the frame of the CR model.

The essence of the stirring effect of the first kind is captured by the pdf's shown in Figure 3 for experiments and in Figure 7 for simulations. Decreasing stirring broadens the pdf and shifts its maxima toward each other. The experimental pdf is Gaussian. The simulations show that this is the case only when averaging

is performed over a sufficiently large number of cells; otherwise, the probability density function is asymmetric. This asymmetry is connected with the interaction of chemical relaxation and feeding processes. The inflow resets the concentration of iodide in a cell from its current value $x_i(t)$ to $x_0 = [I^-]_0$. This concentration increases with time because of chemical reaction. Therefore, $[I^-]_0$ is the smallest concentration that may be observed in any cell, and the pdf is cut off at this value. Each cell evolves from this concentration toward the steady state $[I^-]_{batch}$, given by the condition $f([I^-]) = 0$. Between $[I^-]_0$ and $[I^-]_{batch}$ the pdf reaches its maximum at x_m. As a result, the probability of finding a cell in the region between x_0 and x_m is higher than that of finding it between x_m and $[I]_{batch}$. This leads to the asymmetry of the pdf obtained when averaging is done over a small number of cells. The asymmetry becomes negligible at high stirring rates and low flow rates. Averaging over a large number of cells also leads to a more symmetric pdf, as a consequence of the central limit theorem.[40] The M dependence of the pdf shown in Figure 4 is related to the size of the sampling volume, i.e., of the electrode. It is known that a decrease of the electrode size increases the intensity of the fluctuations of the signal.[22]

While the calculated shift Δ of steady states from their high stirring limits is qualitatively correct, the calculated shifts, particularly of the lower SS2 (cf. Figures 1 and 5), and transition points do not agree quantitatively. The following paper, however, will validate the physical content of the CR model and its suitability, by analyzing the scaling relations between macroscopic shifts of the steady states, stirring rate, and fluctuation amplitude.

Acknowledgment. This work is supported by the Natural Sciences and Engineering Research Council of Canada. We thank Dr. K. Kawagoe of Axon Intstruments Inc. (Foster City, CA) for graciously donating the Pt microelectrodes.

References and Notes

(1) Epstein, I. R. *Nature* **1995**, *374*, 321.
(2) (a) Villermaux, J. In *Spatial Inhomogeneities and Transient Behaviour in Chemical Kinetics*; Gray, P., et al., Eds.; Manchester University Press: New York, 1988, p 119. (b) *Turbulence in Mixing Operations*, Brodkey, R. S., Ed.; Academic Press: New York, 1975. (c) Nauman, E. B.; Buffham, B. A. *Mixing in Continuous Flow Systems*; Wiley: New York, 1983.
(3) Roux, J. C.; De Kepper, P.; Boissonade, J. *Phys. Lett*. **1983**, *A97*, 168.
(4) Luo, Y.; Epstein, I. R. *J. Phys. Chem*. **1986**, *86*, 5733.
(5) Villermaux, J. In *Encyclopedia of Fluid Mechanics*; Gulf Publishers: Houston, 1986; Chapter 27.
(6) Menzinger, M.; Boukalouch, M.; De Kepper, P.; Boissonade, J.; Roux, J. C.; Saadaoui, H. *J. Phys. Chem*. **1986**, *90*, 313.
(7) Dutt, A. K.; Menzinger, M. *J. Phys. Chem*. **1990**, *94*, 4867.
(8) (a) Kondepudi, D. K.; Kaufmann, R. J.; Singh, N. *Science* **1990**, *250*, 975. (b) Metcalfe, G.; Ottino, J. M. *Phys. Rev. Lett*. **1994**, *72*, 2875.
(9) Nitzan, A.; Ortoleva, P.; Deutch, J.; Ross, J. *J. Chem. Phys*. **1974**, *61*, 1056.
(10) Curl, R. L. *AIChE J*. **1963**, *9*, 175.
(11) Kumpinsky, E.; Epstein, I. R. *J. Chem. Phys*. **1985**, *82*, 53.
(12) Ali, F.; Menzinger, M. *J. Phys. Chem*. **1992**, *96*, 1511.
(13) Gyögyi, L.; Field, R. J. *J. Phys. Chem*. **1992**, *96*, 1220.
(14) Gyögyi, L.; Field, R. J. *J. Chem. Phys*. **1989**, *91*, 6131.
(15) Bar-Eli, K.; Noyes, R. M. *J. Chem. Phys*. **1986**, *85*, 3251.
(16) Landau, L. D.; Lifshitz, E. M. *Fluid Mechanics*; Pergamon: London, 1959.
(17) Fox, R. O.; Villermaux, J. *Chem. Eng. Sci*. **1990**, *45*, 2857.
(18) Wendt, J. F. *Computational Fluid Dynamics: An Introduction*; Springer-Verlag: Berlin, 1996.
(19) Ali, F.; Menzinger, M. *J. Phys. Chem*. **1997**, *101*, 2304.
(20) Strizhak, P.; Ali, F.; Menzinger, M. *J. Phys. Chem*. **1999**, *103*, 10866.
(21) Strizhak, P.; Menzinger, M. *J. Phys. Chem*. **1996**, *100*, 19182.
(22) Menzinger, M.; Dutt, A. K. *J. Phys. Chem*. **1990**, *94*, 4510.
(23) Ochiai, E.-I.; Menzinger, M. *J. Phys. Chem*. **1990**, *94*, 8866.
(24) Dutt, A. K.; Muller, S. C. *J. Phys. Chem*. **1993**, *97*, 10059.
(25) De Kepper, P.; Horsthemke, W. *C. R. Acad. Sci*. **1980**, *80*, 4177.
(26) Horsthemke, W.; Lefever, R. *Noise-Induced Transitions*, Springer-Verlag: Berlin, 1984.
(27) Dutt, A. K.; Menzinger, M. *J. Phys. Chem*. **1991**, *95*, 3429.
(28) De Kepper, P.; Epstein, I. R.; Kustin, K. *J. Am. Chem. Soc*. **1981**, *103*, 6121.
(29) Papsin, G. A.; Hanna, A.; Showalter, K. *J. Phys. Chem*. **1981**, *85*, 2575.
(30) Horsthemke, W.; Hannon, L. *J. Chem. Phys*. **1984**, *81*, 4363.
(31) Hannon, L.; Horsthemke, W. *J. Chem. Phys*. **1987**, *86*, 140.
(32) Evangelista, J. J.; Katz, S.; Shinnar, R. *AIChE J*. **1969**, *15*, 843.
(33) Spielman, L. A.; Levenspiel, O. *Chem. Eng. Sci*. **1965**, *20*, 247.
(34) Fox, R. O. *Chem. Eng. Sci*. **1991**, *46*, 1829.
(35) Kattan, A.; Adler, R. J. *AIChE J*. **1967**, *13*, 580.
(36) Pifer, T.; Ganapathisubramanian, N.; Showalter, K. *J. Phys. Chem*. **1985**, *83*, 1101.
(37) Liebhafsky, H. A.; Roe, G. M. *Int. J. Chem. Kinet*. **1979**, *11*, 693.
(38) We assume that system is ergodic; i.e., its ensemble average gives the same result as averaging over time; this is confirmed by an analysis of simulations which shows that the value $\langle x(t)\rangle_M$ does not depend on M.
(39) Nagata, S. *Mixing: Principles and Applications*; John Wiley & Sons: New York, 1975.
(40) Feller, W. *An Introduction to Probability Theory and its Applications*; John Wiley & Sons: New York, 1971.